Theoretical Prediction and Experimental Testing of Mechanical Properties for 3D Printed Silk Fibroin-Type II Collagen Scaffolds for Cartilage Regeneration

Lilan Gao[1, 2, *], Qingxian Yuan[1, 2], Ruixin Li[3, *], Lei Chen[1, 2], Chunqiu Zhang[1, 2] and Xizheng Zhang[1, 2]

Abstract: Silk fibroin-type II collagen scaffold was made by 3D printing technique and freeze-drying method, and its mechanical properties were studied by experiments and theoretical prediction. The results show that the three-dimensional silk fibroin-type II collagen scaffold has good porosity and water absorption, which is (89.3%+3.26%) and (824.09%+93.05%), respectively. With the given strain value, the stress of scaffold decreases rapidly firstly and then tends to be stable during the stress relaxation. Both initial and instantaneous stresses increase with increase of applied strain value. The creep strains of scaffold with different stress levels show the two stages: the rapidly increasing stage and the second stable stage. It is noted that the scaffold with compressive stress of less than 35 kPa can recover when the compressive stress is removed. However when the compressive stress is higher than 50 kPa, the scaffold is damaged and its structure is destroyed. Not only the compressive property but tensile property of scaffold are dependent on the applied displacement rate or strain rate. Its compressive elastic modulus and tensile modulus increase with increase of strain rate or displacement rate. The nonlinear relaxation model and creep model were constructed respectively and applied to predict the stress relaxation behavior and creep behavior of scaffold. It is found that there are good agreements between the experimental data and predictions, which mean that the built theoretical model can predict the mechanical behavior of scaffold.

Keywords: Silk fibroin, type II collagen, cartilage scaffold, low temperature 3D printing technology, constitutive model, mechanical properties.

1 Introduction

Articular cartilage is a kind of highly hydrated tissue without blood or lymphatic vessel tissue. Its self-repair ability after injury is weak due to lack of nutrients supply [Mow, Ratcliffe and Poole (1992)]. There are some problems for the repair of cartilage damage

---

[1] Tianjin Key Laboratory for Advanced Mechatronic System Design and Intelligent Control, School of Mechanical Engineering, Tianjin University of Technology, Tianjin 30000, China.

[2] National Demonstration Center for Experimental Mechanical and Electrical Engineering Education (Tianjin University of Technology), Tianjin300000, China.

[3] Hospital of Stomatolgy, NanKai University, Tianjin300000, China.

* Corresponding author: Lilan Gao. Email: gaolilan780921@163.com; Ruixin Li. Email: limxinxin@163.com.

in the current clinical treatment, such as the shortage of donor tissues and requirement of a secondary surgery. These problems have limited the application of cartilage repair techniques [Zhou, Zhang, Cai et al. (2017)]. The rapid development of tissue engineering provides a promising approach for the repair of cartilage damage with minimally invasive operation.

The choice of materials is one of the focuses of tissue engineering research. At present, a large number of researchers are trying to find a kind of scaffold with good biocompatibility, biodegradability and mechanical properties for cartilage repair. The popular materials are natural materials (mainly chitosan, silk fibroin, type Ⅰ collagen and type Ⅱ collagen), artificial materials (polyglycolated, polylactic acid, polycaprolactone and polyethylene glycol etc.) and composites. Almela et al. [Almela, Brook, Khoshroo et al. (2017)] used 3D printing technology to print bilayer calcium phosphate-based scaffolds to simulate the cortical-cancellous structure of bone with a porosity of $61.8 \pm 1.4\%$. It was found that osteoblasts could grow and proliferate on the scaffold. Zitnay et al. [Zitnay, Reese, Tran et al. (2017)] prepared the high density collagen scaffold with aligned collagen fibrils. It was found that the mesenchymal stem cells proliferated on the scaffold and migrated into the pores of scaffold.

Articular cartilage covers the surface of subchondral bone in diarthrodial joint to transmit loads, absorb shock and sustain daily loading histories. In daily activities, articular cartilage is exposed to a wide range of loads which includes both static and dynamic loads. When the cartilage scaffold, seeded with chondrocytes or cells induces by bMSC, is implanted in cartilage defect, the scaffold is expected to not only grow some cartilaginous tissue inside its pores but also bear loads. The bearing capacity of implant derives from the original mechanical properties of scaffold and the water permeability into the scaffold. Hutmacher proposed that the difference of stress between the scaffold and neighbouring tissue should be diminished [Hutmacher (2000)], and simultaneously the scaffold can supply proper mechanotransduction signals to cells so as to create their ECM [Chiquet, Renedo, Huber et al. (2003)]. Hence the mechanical properties of scaffold are very important.

As we know that the cartilage is able to sustain daily loading histories because of the combination of collagen fiber's stiffness and high water content [Roughley and Lee (1994)]. Collagen type II, as the main organic component of cartilage matrix, plays an important role in the occurrence, differentiation and migration of chondrocytes [Almela, Brook, Khoshroo et al. (2017)]. Silk fibroin is a natural material with good biocompatibility, degradability and mechanical properties. Low-temperature 3D printing technology is a kind of rapid prototyping technology that accumulates materials layer by layer and deposits them into real objects [Moroni, Wijn, van Blitterswijk et al. (2006)].

In this study, we mixed the Collagen type Ⅱ and silk fibroin, and fabricated the silk fibroin-type Ⅱ collagen scaffold by applying low temperature 3D printing technique and freeze-drying method. Based on the printed scaffold its physical parameters were measured. The mechanical behaviors of scaffold were investigated by carrying out the stress relaxation, creep and rate correlation experiments, respectively. Simultaneously, the nonlinear viscoelastic constitutive model was constructed to describe the stress-relaxation behavior and creep property of scaffold.

2 Materials and methods

2.1 Materials

Natural silk and fresh bovine scapula were purchased from Supermarkets (China). Anhydrous calcium chloride and absolute ethyl alcohol were purchased from kermel (China) for dissolving the silk in the extraction process. Sodium carbonate and polyethylene glycol solution were obtained from Solarbio-Beijin (China). Pepsin was purchased from Sigma (USA) for Extraction of type Ⅱ collagen.

2.2 Preparation of fibroin-type II collagen scaffold

2.2.1 Preparation of silk fibroin solution

The natural silk was immersed in the sodium carbonate solution with mass fraction of 0.5% and the mixed solution was boiled for 30 min. The turbid liquid was discarded, and the silk was cleaned, which was repeated 3 times. The dry silk fibroin was dissolved in the $CaCl_2•H_2O•C_2H_5OH$ mixed solution with molar ratio of 1:8:2, and then the silk fibroin solution was stirred with low speed until completely dissolved so far. The silk fibroin solution was dialyzed in the dialysis bag with flow water for 48 h, and then was dialyzed with deionized water for 24 h. The silk fibroin solution after dialysis was concentrated with polyethylene glycol solution, and then was centrifuged so as to discard the supernatant. Finally the prepared silk fibroin solution was sealed and stored at 4°C.

2.2.2 Preparation of type Ⅱ Collagen

The fresh bovine cartilage was carefully cleaned and crushed, then being soaked in ethanol solution for 24 h and being swollen in acetic acid solution containing pepsin for 48 h. The swollen collagen was then centrifuged at 8000 r/min for 10 min at 4°C, and the supernatant acidic collagen solution was neutralized with 0.5 M hydroxide sodium solution and salted out by adding sodium chloride crystals for 2 h. The collagen was removed into dialysis bags and then was dialyzed in deionized water for 4 d. It is noted that the deionized water was changed every 4 h. Collagen after dialysis was kept at 4°C before experiment.

2.2.3 Low temperature 3D printing of composite scaffold

The type Ⅱ collagen and silk fibroin were homogeneously mixed into the colloidal mixture at a mass ratio of 3:7. The mixture was centrifuged to remove the bubbles and then was loaded into a 10 mL syringe (with 1/4 needle). Solidworks software (Dassault Systemes SA, France) was used to design the scaffold model. The model shape and internal aperture are macroscopically square. A silk fibroin-type Ⅱ collagen complex with a lattice structure was prepared by using a low-temperature 3D printer to adjust the printing speed and extrusion speed and freeze-dried for 36 h in a vacuum state. Tab. 1 shows the optimized parameters for printing the scaffold. Fig. 1 presents the diagram of 3D printing process and the cross section profile of scaffold. Fig. 2 shows the appearance diagram of prepared fibroin-type Ⅱ collagen cartilage scaffold. The hole spacing of scaffold is 0.8 mm and the thickness of each layer is 0.25 mm.
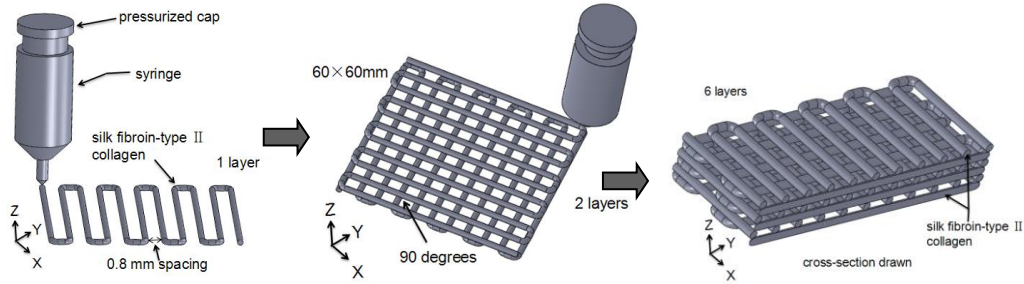
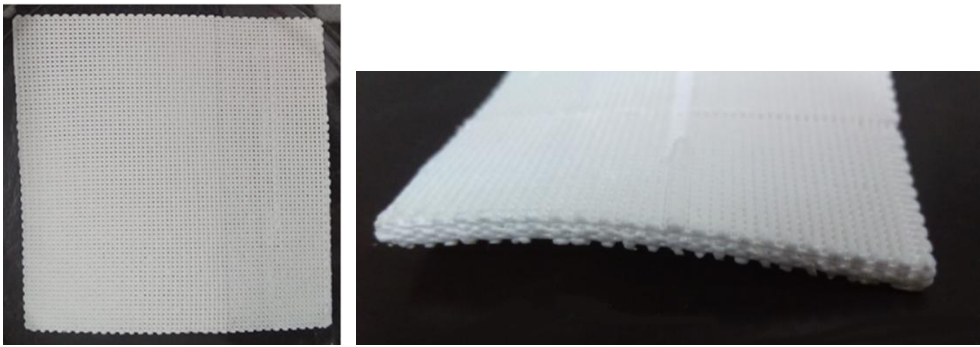**Figure 1:** Diagram of 3D printing process and cross section profile of scaffold

Figure 2: Silk fibroin-type II collagen cartilage scaffold

Table 1: The optimized parameters for printing the scaffold

	Parameter	Measurement
1	Print speed	15 mm/s
2	Material extrusion speed	0.25 mm/min
3	Material temperature	Room temperature
4	Platform temperature	-20°C
5	Scaffold aperture	0.8 mm
6	Thickness	0.25 mm

2.3 Physical properties

The porosity and density of the scaffold sections were measured in a specific gravity bottle (Hubbard, Hanil, Korea) through the ethanol immersion method based on Archimedes' Principle [Park, Kim, Lee et al. (2007)]. The quality of scaffold is denoted as m_0. Briefly, the porosity and density of scaffold were determined as follows:

$$\text{Porosity}(\%) = \frac{(m_2 - m_3 - m_s)/\rho_e}{(m_1 - m_3)/\rho_e} \times 100\% \tag{1}$$

$$\text{Density}(\text{g/cm}^3) = \frac{m_s}{m_2 - m_3 - m_s} \times \rho_e \tag{2}$$

Where m_1 is the specific gravity bottle weight filled with ethanol, m_2 is the specific gravity bottle weight filled with ethanol and scaffold, m_3 is the weight of the specific gravity bottle after taking out the ethanol-saturated scaffold from m_2, and ρ_e is the ethanol density. Therefore, $(m_2 - m_3 - m_s)/\rho_e$ is the total volume of the scaffold including pores, and $(m_1 - m_3)/\rho_e$ is the pore volume in the scaffold [Lai, Cao, Wang et al. (2017)].

Discs of fibroin-type II collagen scaffolds were weighed and then incubated in 50 ml of phosphate-buffered solution (PBS, pH7.4) at 37°C. The scaffolds were removed from the medium, and its wet weight (m_w) was subsequently measured. The swelling ratio of scaffold was calculated as the ratio of increased weight (m_w-m_s) to the initial weight (m_s) according to the following equation:

$$\text{Water absorption}\left(\%\right) = \frac{m_w - m_s}{m_s} \times 100\% \tag{3}$$

The experiment was performed with three samples every group and the average measurement was calculated [Lee and Kamarul (2014)].

2.4 Mechanical tests

The stress relaxation, creep and rate-dependent experiments were performed to investigate the mechanical properties of scaffold by using a Instron 5800 Universal testing machine (Instron, USA) with a 100N load sensor. The testing machine is fitted with a flat head for compression and a fixture for stretching [Vikingsson, Claessens, Gómez-Tejedor et al. (2015); Ratakonda, Sridhar, Rhinehart et al. (2012); Jelen, Mattei, Montemurro et al. (2013)], which is shown in Fig. 3. Before and after the experiment, the samples were immersed in PBS buffer of pH7.4 to ensure that the samples were always in wet state during the experiments.

2.4.1 Stress relaxation test

The scaffold sample was placed on the stainless steel platform of mechanical test machine, and the loading was started when the flat head was lightly contacted with the sample. The compressive strains of 10%, 20% and 30% were applied to the scaffold sample at constant speed of 0.05%/s, 0.5%/s and 5%/s, and then were preserved constant during the relaxation time (t=30 min) at room temperature respectively. Three samples of each group were tested considering random error. All stress-time data were recorded automatically by machine and the stress-time graph was drawn. After unloaded completely, the samples were immersed in PBS buffer in order to analyze their recovery.
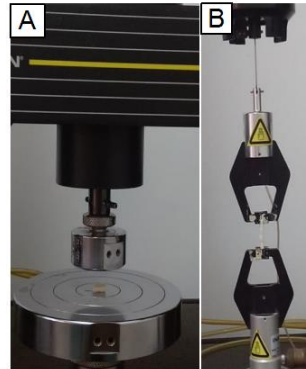
Figure 3: Compression device (A) and stretching device (B) of Instron 5800 universal testing machine

2.4.2 Creep test

The creep tests were conducted at given stress levels under unconfined compression for scaffold specimens. The constant compressive stress levels of 5 kPa, 20 kPa, 35 kPa and 50 kPa were applied on four sets of independent samples at room temperature respectively and the creep time is 60 min. Three samples of each group were tested. The strain was recorded automatically during the whole creep process of the material and the strain-time graph was drawn for each stress level. Similarly, after unloaded completely, the samples were immersed in PBS buffer in order to analyze their recovery.

2.4.3 Rate-dependent test

The uniaxial compressive experiment and tensile experiment were carried out for scaffold samples so as to investigate its rate dependence, respectively. Under uniaxial compression the scaffold samples were compressed to strain of 30% with different strain rates such as 0.05%/s, 0.5%/s and 5%/s. Under tensile load the samples were stretched to fracture with different displacement rates of 0.1 mm/min, 1 mm/min, 10 mm/min, respectively. It is probed for the rate-dependent performance of scaffold including elastic modulus and tensile strength.

3 Theoretical models

3.1 Nonlinear relaxation model

The constitutive relationship of a kind of nonlinear viscoelastic material under uniaxial loading obeys the following constitutive equation proposed by Drozdov [Drozdov and Dorfmann (2004)]:

$$\sigma(t) = [1 - Q_*(t)]\Phi(\varepsilon(t)) + \int_0^t \bar{Q}_*(t-s)\Phi(\varepsilon(t) - \varepsilon(s))ds \qquad (4)$$

Where σ is the stress, ε is the strain, Q_* and $\bar{Q}_*$ are the relaxation measure and its differentiation with respect to time t, $\Phi(\varepsilon)$ is the given function which characterizes

the material's nonlinearity

For the standard relaxation test under constant strain value the constitutive Eq. (4) can yield

$$\sigma_s(t) = [1 - Q_*(t)]\Phi(\varepsilon) \tag{5}$$

The relaxation measure Q_* is determined by the number M of different classes of links and material parameters $\mu^{(m)}$ and $\gamma^{(m)}$, and can be expressed as

$$Q_*(t) = \sum_{m=1}^{M} \mu^{(m)}\left[1 - e^{-\gamma^{(m)}t}\right] \tag{6}$$

The given function $\Phi(\varepsilon)$ is obtained from Eq. (5) and Eq. (6) when the time tends to zero as shown in the following.

$$\Phi(\varepsilon) = \sigma_s(0) \tag{7}$$

By putting Eq. (6) and Eq. (7) into Eq. (5), the nonlinear relaxation model can be derived as

$$\sigma_s(t) = \left[1 - \sum_{m=1}^{M} \mu^{(m)}\left(1 - e^{-\gamma^{(m)}t}\right)\right] \cdot \sigma_s(0) \tag{8}$$

For cartilage scaffold the number M is supposed to 2 based on the temperature scan of heat flux obtained through the differential scanning calorimetry (DSC) for cartilage collagen. The material constants $\mu^{(m)}$ and $\gamma^{(m)}$ are found by fitting experimental data for scaffold in stress relaxation tests with constant strain values based on the Eq. (8). Thus the stress relaxation behaviors of scaffold with different strain values can be predicted based on the Eq. (8).

3.2 Nonlinear creep model

The scaffold can be described by the nonlinear viscoelastic constitutive model by Lou and Schapery considering its nonlinear viscoelastic characteristic [Lou and Schapery (1969)]. The stress-strain equation for uniaxial loading can be expressed as

$$\varepsilon = g_0 A(0)\sigma + g_1 \int_0^t \Delta A(\psi - \psi') \frac{dg_2\sigma}{d\tau} d\tau \tag{9}$$

Where $A(0)$ and $\Delta A(\psi)$ are the initial and transient components of linear viscoelastic creep compliance, respectively. t is the loading time. g_0, g_1, g_2 are the stress-dependent material parameters and their changes reflect the third and higher order stress-dependence of Gibbs free energy. ψ is the converted time and is expressed as

$$\psi = \psi(t) = \int_0^t \frac{dt'}{a_\sigma}, \quad \psi' = \psi(\tau) = \int_0^\tau \frac{dt'}{a_\sigma} \tag{10}$$

Here a_σ is the time-scale factor, which reflects the relevance of free energy, stress and

temperature. In this study we assume that a_σ depends only on the applied stress.

For creep deformation under constant stress, the Eq. (9) yields

$$\varepsilon = g_0 A(0)\sigma + g_1 g_2 \Delta A(\frac{t}{a_\sigma})\sigma \tag{11}$$

The creep strain of many materials with constant stress obeys a power law relation. Thus the transient component of linear viscoelastic creep compliance is expressed as

$$\Delta A(\psi) = C\psi^n \tag{12}$$

Where C is the creep constant. n is the creep index.

By substituting Eq. (12) into Eq. (11), we obtain the nonlinear viscoelastic creep model

$$\varepsilon = g_0 A(0)\sigma + C\frac{g_1 g_2}{a_\sigma^n}t^n\sigma \tag{13}$$

The nonlinear creep compliance is defined in the same way as the linear viscoelastic compliance, which is the ratio of strain and stress in creep test, as shown below.

$$A_\theta = \frac{\varepsilon}{\sigma} \tag{14}$$

By combining the Eq. (13) and Eq. (14), the equation of nonlinear viscoelastic creep compliance is obtained

$$A_\theta = g_0 A(0) + C\frac{g_1 g_2}{a_\sigma^n}t^n \tag{15}$$

Where $g_0 A(0)$ is the initial component of nonlinear viscoelastic creep compliance or the initial creep compliance for short, and is calculated by using $g_0 A(0) = \varepsilon_0 / \sigma$. By using the least square method the relationship between the initial creep compliance and stress for cartilage scaffold is acquired as shown in Eq. (16). $C\frac{g_1 g_2}{a_\sigma^n}$ is the nonlinear viscoelastic creep coefficient. n is the creep index.

$$g_0 A(0) = 4.27\sigma^{-0.28} \tag{16}$$

After transforming the Eq. (15) we take the logarithm and obtain

$$\log[A_\theta - g_0 A(0)] = \log \Delta A = n\log t + \log(C\frac{g_1 g_2}{a_\sigma^n}) \tag{17}$$

Where ΔA is the net component of nonlinear viscoelastic creep compliance and is calculated by using $\Delta A = \frac{\varepsilon - \varepsilon_0}{\sigma}$. It is found that there is the linear relationship between ΔA and t in log-log coordinate. The slope of straight line is the n and its vertical intercept is the logarithm of creep coefficient. We can find that n is independent on the applied stress and is 0.26. The relationship between the creep coefficient and stress is

fitted as

$$C\frac{g_1 g_2}{a_\sigma^n} = -0.001\sigma + 0.08 \tag{18}$$

Thus the creep strain of scaffold with different stress levels can be predicted based on the Eqs. (13), (16) and (18). The creep compliance with different stress levels can be predicted based on the Eqs. (15), (16) and (18).

4 Results and discussions

4.1 Physical property of scaffold

The density, porosity and water absorption of the silk fibroin-type II collagen scaffold were calculated, as shown in Tab. 2. It can be seen that the density of the scaffolds is (0.0866 ± 0.0084) g/cm^3, the porosity is $89.3\%\pm3.26\%$ and the water absorption is $824.09\%\pm93.05\%$.

Table 2: Physical properties of scaffold

	Parameter	Measurement
1	Density (g/cm^3)	0.0866±0.0084
2	Porosity (%)	89.3±3.26
3	Water absorption (%)	824.09±93.05

4.2 Stress relaxation behavior of scaffold with different strain values

Fig. 4 shows the stress relaxation curves of scaffold with different strain values when applying the constant compression rate of 0.5%/s, which was obtained by experiments. It is found that the stress of scaffold decreases rapidly with the relaxation time, and then decreases slowly. Not only the initial stress but also the instantaneous stress increase with increase of applied strain. When the compressive strain is 10%, 20% and 30%, the corresponding initial stress values are 5.22 kPa, 9.31 kPa and 14.70 kPa respectively and the initial relaxation rates are 4.59 kPa/min, 2.94 kPa/min and 1.88 kPa/min respectively. The main reason is that the three-dimensional space structure of scaffold and the solution contained in the scaffold have significant effects on the compression behaviors of scaffold. In 2012, we studied the stress relaxation behaviors of articular cartilage with different compressive strains and the results agree with the results of scaffold in the present study [Gao, Zhang, Dong et al. (2012); Gao, Zhang, Gao et al. (2014)].

The stress relaxation behaviors of scaffolds with different strain values were predicted by the relaxation model constructed in this study. It is found that the predictions agree with the experimental data very well as shown in Fig. 4.
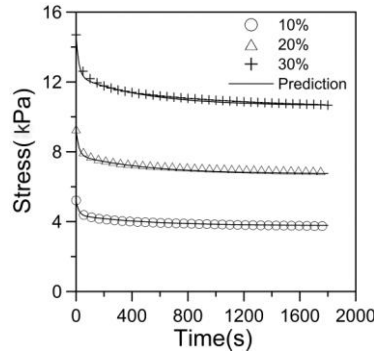
Figure 4: Stress relaxation curves of scaffolds under different compression strains by experiments and predictions

4.3 Creep behavior of cartilage scaffold with different stress levels

Fig. 5 shows the creep curves of scaffold with different compression stress levels and the comparisons between the experimental data and predictions. The results show that the creep strains with different stress levels increase as creep time going on and can be divided in two stages. The creep strain increases rapidly in the initial stage (within 500 s) and then increases at a small rate. We can find that the strain curves with different stress levels after 500 s become flatter and flatter. It is noted that the scaffold with the larger compressive stress become thinner after unloading. When the applied stress is 50 kPa, the scaffolds are extruded as the thin slice. The structure of scaffold is destroyed, especially. The scaffolds with stress level of 5 kPa can recover immediately when being soaked in the PBS of pH7.4. It takes a period of time for the scaffolds with stress levels of 20 kPa and 35 kPa to recover completely in the PBS of pH7.4, while the scaffolds under 50 kPa only can partly recover.
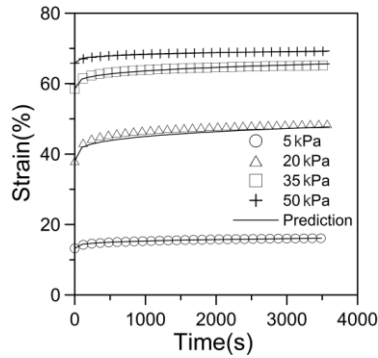

Figure 5: Creep strains of scaffold under different stress levels by experiments and predictions
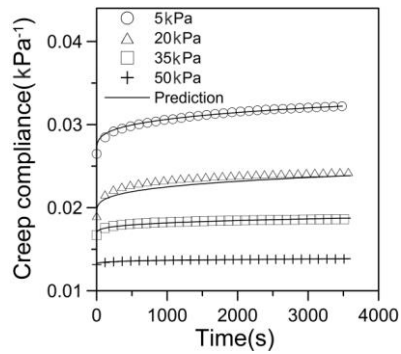
Figure 6: Creep compliance of scaffold under different stress levels by experiments and predictions

Fig. 6 shows the creep compliance of scaffolds with different stress levels. It is found that

the creep compliance decreases with increase of stress levels. The creep compliance of scaffold with stress levels of 5 kPa and 20 kPa increases slowly with time, while the creep compliance with stress level of 50 kPa changes little, which may be due to the destruction of scaffold structure.

Simultaneously the creep strain and creep compliance of scaffolds were predicted by the creep model built in this study. Figs. 5 and 6 show that there are agreements between the predictions and experimental data.

4.4 Mechanical behaviors of scaffold with different strain or displacement rates

The mechanical behaviors of scaffold were investigated with different rates under axial compressive loading and tensile loading, respectively. Fig. 7 shows the stress-strain curves of scaffold at different compression rates and it is found that the stress-strain curves are not coincident, which means that the scaffold is a kind of rate-dependent viscoelastic material. The compressive stress of scaffold with the same compressive strain increases with strain rate rising. The compressive elastic modulus of scaffold also increases with increase of strain rate, which are 34.97 kPa, 45.98 kPa and 49.97 kPa, respectively, as shown in Fig. 8. Younesi et al. [Younesi, Goldberg and Akkus (2015)] made a kind of macroporous collagen scaffold, which was crosslinked in genipin solution, and it is found that the elastic modulus of the scaffold is 0.83±0.39 MPa, and the porosity is 80%. It is noted that the scaffold was prepared by low temperature 3D printing technology and the genipin solution was not used in this study. So its elastic modulus is relatively small, and however its porosity is relatively high.
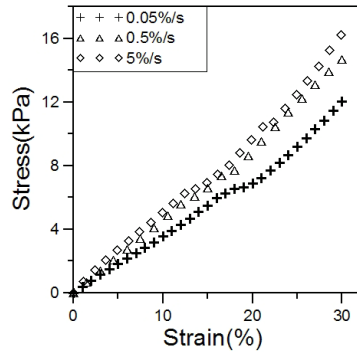

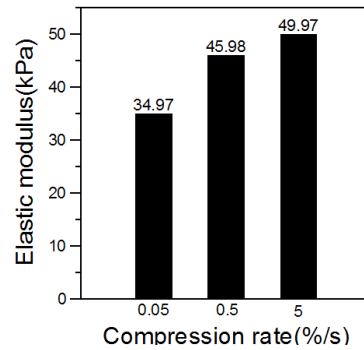**Figure 7:** Stress-strain curves of scaffold at different compression rates

Figure 8: Elastic modulus of scaffold at different compression rates

Fig. 9 shows the stress-strain curves of scaffold at different tensile rates. The results show that the tensile mechanical properties of scaffold are also rate-dependent. The tensile strength, which is the stress value when scaffold is fractured, is 12.85 kPa, 17.13 kPa and 18.54 kPa at displacement rates of 0.1 mm/min, 1 mm/min and 10 mm/min, respectively. It means that the tensile strength of scaffold increases with displacement rate increasing. However the fracture strain decreases gradually, which is 17.59%, 14.64% and 10.38%, respectively. With increase of displacement rate, the elastic modulus increases gradually, which is 70.55 kPa, 115.2 kPa and 179.3 kPa, respectively, as shown in Fig. 10. It is also

noted that the tensile modulus of the scaffold was larger than its compressive elastic modulus.
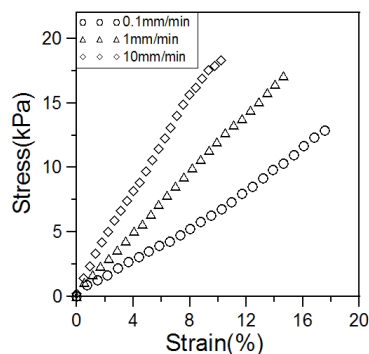

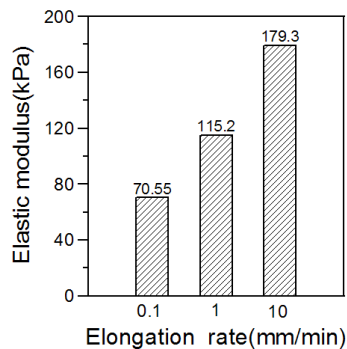**Figure 9:** Stress-strain curves of scaffold at different tensile rates

Figure 10: Elastic modulus of scaffold at different tensile rates

5 Conclusions

Three-dimensional silk fibroin -II collagen scaffold prepared in this study has good connectivity, which is a kind of nonlinear viscoelastic material. The stress of scaffold decreases rapidly in the initial stage, then decreases slowly, and finally tends to be stable during the stress relaxation process. The creep strain of scaffold increases with increasing of compressive stress. The scaffold with compressive stress of 5 kPa and 20 kPa can recover in PBS buffer after unloading, and however the scaffold structure is damaged when the load is higher than 50 kPa. Both compressive properties and tensile properties of scaffold are dependent on the applied strain rate or displacement rate. The compressive elastic modulus or tensile elastic modulus increases with increase of strain rate. The built relaxation model and creep model can predict the mechanical properties of scaffold very well.

Conflict of interest statement: There are no conflicts of interest for either author.

References

Almela, T.; Brook, I. M.; Khoshroo, K.; Rasoulianboroujeni, M.; Fahimipour, F. et al. (2017): Simulation of cortico-cancellous bone structure by 3D printing of bilayer calcium phosphate-based scaffolds. *Bioprinting*, vol. 6, pp. 1-7.

Chiquet, M.; Renedo, A. S.; Huber, F.; Flück, M. (2003): How do fibroblasts translate mechanical signals into changes in extracellular matrix production? *Matrix Biology*, vol. 22, no. 1, pp. 73-80.

Drozdov, A. D.; Dorfmann, A. (2004): A constitutive model in finite viscoelasticity of

particle-reinforced rubbers. *Meccanica*, vol. 39, no. 3, pp. 245-270.

Gao, L. L.; Zhang, C. Q.; Dong, L. M.; Jia, Y. W. (2012): Description of depth-dependent nonlinear viscoelastic behavior for articular cartilage in unconfined compression. *Materials Science & Engineering C*, vol. 32, no. 2, pp. 119-125.

Gao, L. L.; Zhang, C. Q.; Gao, H.; Liu, Z. D.; Xiao, P. P. (2014): Depth and rate dependent mechanical behaviors for articular cartilage: Experiments and theoretical predictions. *Materials Science & Engineering C*, vol. 38, no. 9, pp. 244-251.

Hutmacher, D. W. (2000): Scaffolds in tissue engineering bone and cartilage. *Biomaterials*, vol. 21, no. 24, pp. 2529-2543.

Jelen, C.; Mattei, G.; Montemurro, F.; De Maria, C.; Mattioli-Belmonte, M. et al. (2013): Bone scaffolds with homogeneous and discrete gradient mechanical properties. *Materials Science & Engineering C*, vol. 33, no. 1, pp. 28-36.

Lai, Y.; Cao, H.; Wang, X.; Chen, S.; Zhang, M. et al. (2018): Porous composite scaffold incorporating osteogenic phytomolecule icariin for promoting skeletal regeneration in challenging osteonecrotic bone in rabbits. *Biomaterials*, vol. 153, pp. 1-13.

Lee, S. Y.; Kamarul, T. (2014): N-O, carboxymethyl chitosan enhanced scaffold porosity and biocompatibility under e-beam irradiation at 50 kgy. *International Journal of Biological Macromolecules*, vol. 64, no. 2, pp. 115-122.

Lou, Y. C.; Schapery, R. A. (1969): Viscoelastic characterization of a nonlinear fiber-reinforced plastic. *Journal of Composite Materials*, vol. 5, no. 2, pp. 208-234.

Moroni, L.; de Wijn, J. R.; van Blitterswijk, C. A. (2006): 3D fiber-deposited scaffolds for tissue engineering: Influence of pores geometry and architecture on dynamic mechanical properties. *Biomaterials*, vol. 27, no. 7, pp. 974-985.

Mow, V. C.; Ratcliffe, A.; Poole, A. R. (1992): Cartilage and diarthrodial joints as paradigms for hierarchical materials and structures. *Biomaterials*, vol. 13, no. 2, pp. 67-97.

Park, I. K.; Kim, J. M.; Lee, J. H.; Oh, S. H. (2007): In vitro and in vivo characteristics of PCL scaffolds with pore size gradient fabricated by a centrifugation method. *Biomaterials*, vol. 28, no. 9, pp. 1664-1671.

Ratakonda, S.; Sridhar, U. M.; Rhinehart, R. R.; Madihally, S. V. (2012): Assessing viscoelastic properties of chitosan scaffolds and validation with cyclical tests. *Acta Biomaterialia*, vol. 8, no. 4, pp. 1566-1575.

Roughley, P. J.; Lee, E. R. (1994): Cartilage proteoglycans: structure and potential functions. *Microscopy Research & Technique*, vol. 28, no. 5, pp. 385.

Sun, W.; Lal, P. (2002)**:** Recent development on computer aided tissue engineering-A review. *Computer Methods & Programs in Biomedicine*, vol. 67, no. 2, pp. 85-103.

Vikingsson, L.; Claessens, B.; Gómez-Tejedor, J. A.; Ferrer, G. G.; Ribelles, J. L. G. (2015): Relationship between micro-porosity, water permeability and mechanical behavior in scaffolds for cartilage engineering. *Journal of the Mechanical Behavior of Biomedical Materials*, vol. 48, pp. 60-69.

Yoo, D. J. (2011): Computer-aided porous scaffold design for tissue engineering using triply periodic minimal surfaces. *International Journal of Precision Engineering &*

Manufacturing, vol. 12, no.1, pp. 61-71.

Younesi, M.; Goldberg, V. M.; Akkus, O. (2015): A micro-architecturally biomimetic collagen template for mesenchymal condensation based cartilage regeneration. *Acta Biomaterialia*, vol. 30, pp. 212-221.

Zhou, F.; Zhang, X.; Cai, D.; Li, J.; Mu, Q. et al (2017): Silk fibroin-chondroitin sulfate scaffold with immuno-inhibition property for articular cartilage repair. *Acta Biomaterialia*, vol. 63, pp. 64-75.

Zitnay, J. L.; Reese, S. P.; Tran, G.; Farhang, N.; Bowles, R. D. et al. (2017): Fabrication of dense anisotropic collagen scaffolds using biaxial compression. *Acta Biomaterialia*, vol. 65, pp. 76-87.